Journal of Analytical and Applied Pyrolysis 181 (2024) 106628

Contents lists available at ScienceDirect

Journal of Analytical and Applied Pyrolysis

journal homepage: www.elsevier.com/locate/jaap

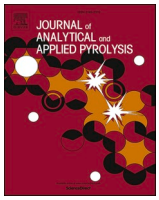

On the role of hydrogen inhibition in gas-phase methane pyrolysis for carbon capture and hydrogen production in a tubular flow reactor

Ahmet Çelik, Akash Bhimrao Shirsath, Fatjon Syla, Heinz Müller, Patrick Lott *, Olaf Deutschmann

Institute for Chemical Technology and Polymer Chemistry (ITCP), Karlsruhe Institute of Technology (KIT), Engesserstr. 20, Karlsruhe 76131, Germany

ARTICLE INFO

Keywords:
Hydrogen production
Methane pyrolysis
Inhibition
Pressure influence
Reaction mechanism

ABSTRACT

The thermal pyrolysis of methane enables economically competitive hydrogen production without direct CO_2 emissions. Although several mechanisms for the process have already been proposed, especially the inhibitory effect of hydrogen as well as the process operation at increased pressure have not yet been fully clarified. In this context, the present work investigates the influence of hydrogen and argon as inert gas on product composition, methane conversion, and hydrogen selectivity as a function of temperature (1000 °C to 1600 °C), residence time (1 s to 7 s), molar dilution ratio (1:1–4:1), and pressure (1 bar to 4 bar) in a high-temperature reactor. Within the scope of this work, total differences in CH_4 conversion of up to 50 % could be observed at equal process parameters between an argon and hydrogen dilution, underlining the potential impact of diluents on the overall process. Moreover, increasing the pressure from 1 bar to 4 bar reduces the formation of byproducts significantly for both H_2 and Ar as diluent, however, with different mechanistic characteristics. The most remarkable difference is the formation of propylene that exclusively takes place in argon-diluted reaction gas mixtures. This occurrence persists unabated, even under elevated pressures and temperatures reaching as high as 1600 °C. We ascribe this phenomenon to the interaction of methyl and ethyl radicals, establishing it as an impasse to further reactions leading to the formation of solid products. Herewith, the study provides novel insights from a reaction engineering perspective as well as from a process development perspective and clarifies the role of the dilution gases hydrogen and argon on the methane pyrolysis reaction.

1. Introduction

Large-scale production of climate-friendly hydrogen (H_2) that can be used as both an energy carrier as well as a chemical feedstock is considered to be a prerequisite for establishing an emission-free chemical industry [1–7]. In this context, methane (CH_4) pyrolysis, during which methane (CH_4) is decomposed into solid elemental carbon (C) and gaseous hydrogen, as shown in Eq. 1, allows for large-scale hydrogen production without direct CO_2 emissions and with a significantly lower energy demand compared to water electrolysis [8–16].

$$CH_{4\,(g)} \rightarrow C_{\,(s)} + 2\,H_{2\,(g)} \quad (1)$$

If the feedstock herein originates from renewable sources such as biogas the process may even serve as a CO_2 sink [17]. The global reaction equation cannot truly represent the magnitude of the individual molecular steps taking place during the endothermic pyrolysis process. These elementary reactions involve the formation of methyl radicals, which are coupled to form ethane (C_2H_6), which is further dehydrogenated to ethylene (C_2H_4) and acetylene (C_2H_2) and thus results in H_2 release. The coupling of C_2H_2 molecules to benzene (C_6H_6) represents the first step for the formation of polycyclic aromatic hydrocarbons (PAH), which in turn act as precursors for the formation of solid carbon, i.e. in the form of graphite or soot [9,18–24]. Notably, C_2H_6, C_2H_4, C_2H_2, or C_6H_6 do not only act as intermediates, but can also appear as byproducts in case of an incomplete reaction.

From a technical point of view, thermal pyrolysis requires temperatures above 1000 °C to realize relevant methane conversions at moderate residence times [9,17,25]. Notably, thermo-catalytic flow tubes [9,17,21,24] enjoy particular interest in academia and industry, even though iron- or nickel-based catalysts allow for technically relevant CH_4 conversions and H_2 selectivities of up to 95 % and more than 80 %, respectively, already at temperatures around 600 °C – 800 °C, and also

* Corresponding author.
E-mail address: patrick.lott@kit.edu (P. Lott).

https://doi.org/10.1016/j.jaap.2024.106628
Received 14 January 2024; Received in revised form 19 May 2024; Accepted 2 July 2024
Available online 3 July 2024

catalytically active molten salt bubble columns enable reasonable conversion already at temperatures of approx. 1000 °C [26–28]. In this context, however, a limited catalyst lifetime due to carbon deposition and potential impurities in the carbon product are significant drawbacks, especially because the utilization of carbon is considered as key factor for the competitiveness of the process [10]. Since these aspects are irrelevant during thermal pyrolysis processes, purer carbon may be preferred despite higher temperature demand and thus energy costs. In this regard, a recent study of our group proposed a model that can predict soot formation; for this, numerical simulations were coupled with experimental characterization using Raman spectroscopy, transmission electron microscopy (TEM), and dynamic light scattering (DLS) [24]. Herein, agglomerated primary particles around 150 nm in diameter were found as solid product and both crystalline and amorphous domains were observed in the soot samples.

When establishing the pyrolysis process on a technical level, the formation of solid carbon in the two-phase reaction system must be controlled in order to avoid undesired pressure increases in the reactor due to carbon deposition-induced clogging. For this, diluent gases such as inert gases or H_2 are commonly used, with the latter being especially attractive as it is already part of the product stream, which makes a downstream separation from the gaseous product stream redundant [9]. For instance, Rokstad et al. [29] investigated the pyrolysis of methane using H_2 or helium as diluent gas and examined the dependence of the product composition on the residence time in detail. However, the study focused mainly on the formation of C_2H_4, C_2H_2, and C_6H_6, which is why comparatively short residence times of less than 1 s were investigated since these minimize the formation of solid carbon. In this context, it has been observed several times that the use of H_2 as a diluent gas influences the kinetics and inhibits the formation of solid carbon on the one hand and enhances the formation of C_2 species on the other hand [29–32].

As a consecutive step towards the realization of an ecologically and economically competitive process, our present work elaborates the influence of hydrogen and argon (Ar) as diluent during methane pyrolysis. For this, experiments in a high-temperature reactor are conducted while varying temperature, pressure, and residence time in order to minimize the byproduct levels and maximize the purity of H_2. Supplemented by thermodynamic equilibrium calculations, this work provides guidance for optimizing the dilution during methane pyrolysis, which can ultimately be exploited when designing an industrial process.

2. Material and methods

The experiments for this study were conducted in an in-house developed setup that was designed for experiments at high temperature and elevated pressure and which was already introduced in previous publications of our group [9,17,33]. It essentially consists of a gas dosing system that feeds the reaction gases (provided by gas bottles), a tubular α-Al_2O_3 reactor (length = 100 cm, diameter = 2 cm; DEGUSSIT AL23 by Friatec/Aliaxis) that can be heated up to 1800 °C by electric heating elements and that is placed in an insulated stainless-steel vessel to ensure a safe operation even in the case of pressurized reactions. The effluent product gas stream was continuously analyzed with a mass spectrometer (MS; Hiden Analytical HPR 20 R&D). While a trap downstream of the reactor allowed to capture the majority of solid particles, an additional particle filter prior to the analysis section removed also fine soot particles. A schematic flow diagram (along with images of carbon deposits) is given in Fig. 1.

During the flow reactor experiments (20 min), the reaction gases were diluted with either H_2 or Ar. Afterwards, the reactor was always purged with Ar. Subsequently, carbon particles and agglomerates that were captured in the carbon trap were removed and deposits that formed during the pyrolysis reaction in the reactor were burned off with synthetic air so that another experiment could be performed. The burn-off process was monitored by continuously analyzing the CO and CO_2 mole fractions via online mass spectrometry and the burn-off was assumed to be completed once no CO and CO_2 could be detected end-of-pipe anymore.

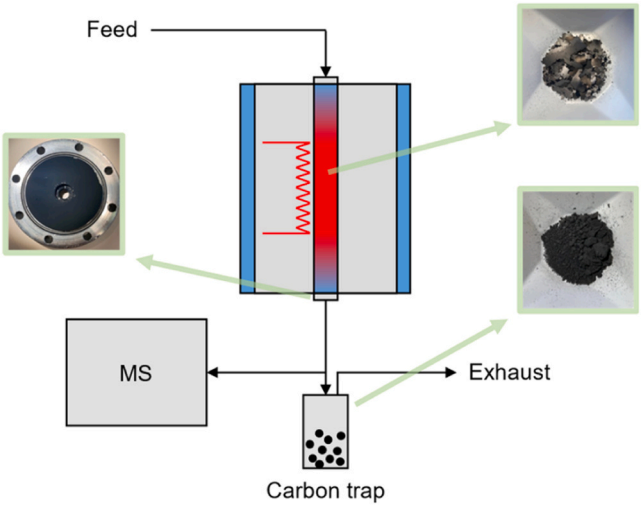

Fig. 1. Schematic flow diagram of the experimental setup with different types of solid carbon accruing during gas-phase CH_4 pyrolysis, depending on the location in the setup.

Note that the characterization of the carbon accruing during the experiments is beyond the scope of the present study. Earlier research from our group already elucidated different carbon formation pathways that explain the different carbon types forming during the flow reactor experiments conducted herein [9,24,34]. On the one hand, soot particles form and agglomerate, which accumulate at the reactor outlet and in the carbon trap; on the other hand, carbon deposition reactions take place particularly on the reactor walls that result in graphite-like carbon (c.f. Fig. 1).

For data evaluation, the molar flow rate of the product stream was calculated via H balance (considering gas expansion) and then multiplied with the respective mole fraction to calculate the flow rate of each species in the product stream. With the latter CH_4 conversion as well as H_2 selectivity was calculated (definition of each given in SI).

The thermodynamic equilibrium analysis was performed using the DETCHEM software package [35]. Herein, $DETCHEM^{EQUIL}$ calculated the equilibrium composition for a specified feed gas mixture based on the thermodynamic potential under isothermal and isobaric conditions. The equilibrium calculations are performed considering carbon formation with graphite as its energetically most favorable form. For comparison, calculated equilibrium data with and without carbon formation is given in the SI. For the calculations, the ideal gas thermodynamic data in polynomial form is used [36]. In addition, the Gibbs free energy ($\Delta_R G$) and the equilibrium constant (K_p) were also calculated for the considered temperatures (definition of both given in SI).

3. Results and discussion

The reaction mechanism of methane pyrolysis involves a variety of side reactions that produce hydrocarbon species as intermediates, making a thermodynamic study crucial. Herein, we have conducted a thermodynamic analysis, depicted in Fig. 2, as a function of temperature for various reactions involving intermediate species such as C_2H_2, C_2H_4, C_6H_6, $C_{10}H_8$, $C_{14}H_{10}$, and $C_{16}H_{10}$, that were identified as particularly significant in previous studies [9,21,24,34].

The Gibbs free energy analysis (Fig. 2a) indicates that the decomposition of CH_4 to carbon (with graphite as the energetically most favorable form) and H_2 begins at approx. 500 °C. However, reactions leading to the formation of intermediate species are thermodynamically favored only above 900 °C. Furthermore, it is evident that the equilibrium constant K_p (Fig. 2b) for reactions involving the formation of PAHs

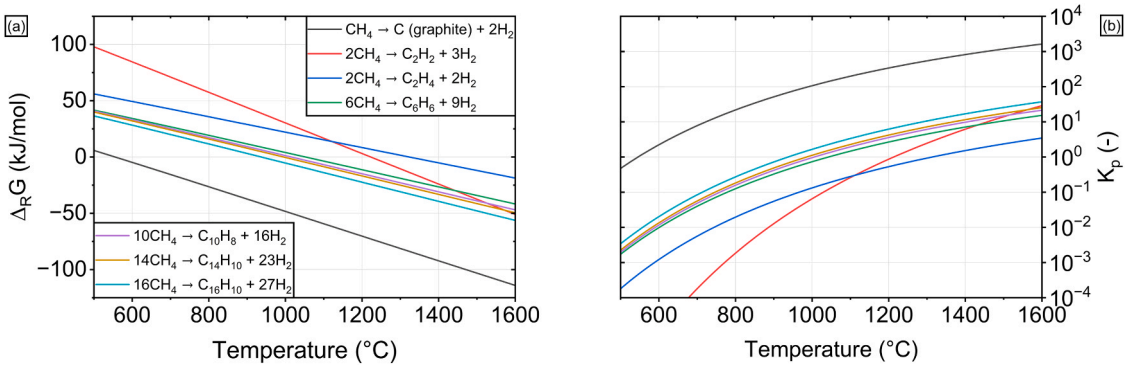

Fig. 2. Thermodynamic analysis of the methane pyrolysis process. Gibbs free energy (a) and equilibrium constant (b) as function of temperature.

such as $C_{10}H_8$, $C_{14}H_{10}$, and $C_{16}H_{10}$, is higher compared to those involving the formation of smaller hydrocarbons like C_2H_2 and C_2H_4. Lastly, the thermodynamic analysis indicates that temperatures above 1000 °C favor the pyrolysis of CH_4.

Consequently, using H_2 or Ar as diluent gas, the influence of temperature T (1000 °C to 1600 °C), residence time τ (1 s to 7 s), molar dilution ratio (1:1–4:1), and pressure p (1 bar to 5 bar) on the product composition during gas-phase CH_4 pyrolysis was worked out, which allows for a process optimization in terms of CH_4 conversion and H_2 selectivity.

3.1. Influence of temperature

Fig. 3 shows the main product (Fig. 3a, b) and byproduct (Fig. 3c, d) levels for a H_2-diluted (left) and an Ar-diluted (right) reaction gas mixture as a function of temperature at constant residence time (5 s), constant pressure (1 bar), and constant molar dilution ratio (2:1). In addition, the results of the corresponding equilibrium calculations are plotted as reference. Note, that for the H_2-diluted data the H_2 levels shown in the graph are the sum of the H_2 amount added as diluent and the amount of H_2 that is produced during the reaction.

For a H_2-diluted mixture, the thermodynamic equilibrium predicts an almost exclusive presence of H_2 and carbon, whereas CH_4 concentrations are essentially irrelevant over the entire temperature range (Fig. 3a). Experimental CH_4 mole fractions approach their respective equilibrium value with increasing temperature until almost full CH_4 conversion is achieved at temperatures above 1400 °C. With regard to the H_2 mole fractions, the experimentally determined values exceed the respective equilibrium values already at 1200 °C. This results from the fact that during the experiments carbon formation does not only proceed via the step-wise dehydrogenation of the gas-phase intermediate species mentioned above, but the gas-phase species are also consumed to form solid carbon via irreversible reactions according to Eq. 2 [34].

$$C_xH_{2y} \rightarrow x\ C + y\ H_2 \quad (2)$$

The overall mass of the gas-phase is hereby reduced, which shifts the equilibrium towards H_2 formation. Similarly, the equilibrium calculations do not predict relevant levels of gas-phase hydrocarbon species, whereas maximum molar fractions of approx. 0.25 % C_2H_2 at 1200 °C, 0.14 % C_2H_6 at 1400 °C, and 0.11 % C_6H_6 at 1200 °C are found during the experiments (Fig. 3c).

For the Ar-diluted gas mixture, qualitatively similar trends can be observed in the experimental data for CH_4 and H_2, whereas the presence of the inert Ar generally reduces the molar fractions of all other components. Herein, the equilibrium mixture consists equally of H_2 and Ar, whereby CH_4 is fully converted. Notably, during the experiments with Ar dilution formation of up to 0.5 % propylene (C_3H_6) was found, which

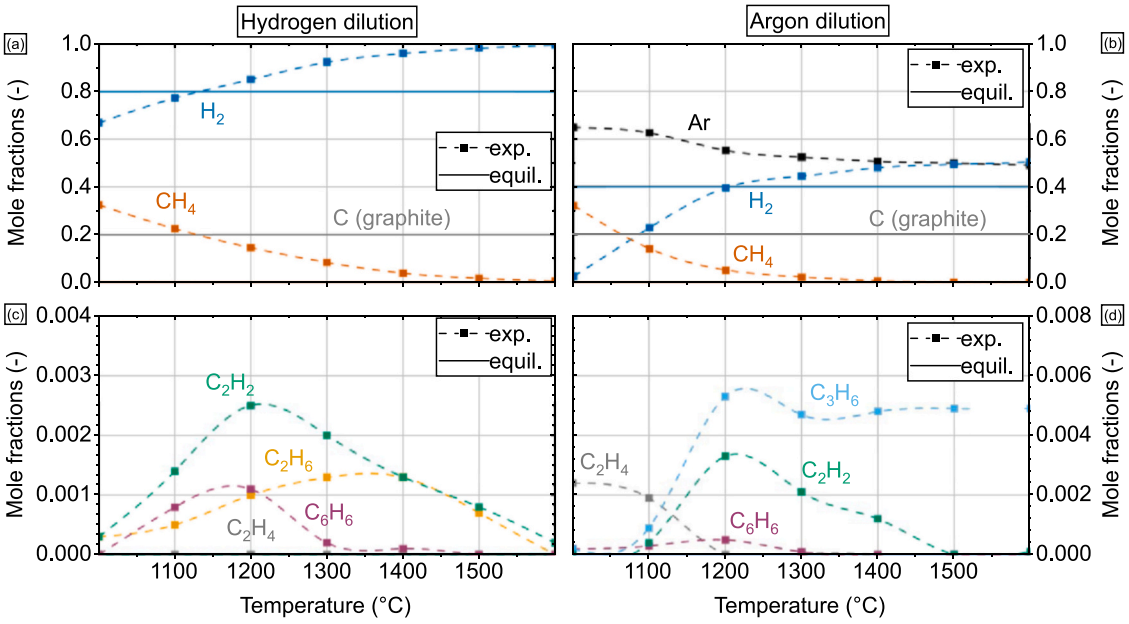

Fig. 3. Main product (a, b) and byproduct (c, d) composition diluted in H_2 (left) or Ar (right) as function of temperature at a residence time of 5 s, a pressure of 1 bar, and a molar dilution ratio of H_2:CH_4 = 2:1 and Ar:CH_4 = 2:1.

cannot be observed in relevant amounts with H_2 dilution.

In order to explain the main qualitative difference between the two diluent gases, namely the formation of propylene even at higher temperatures, H_2 inhibition must be studied at the molecular level. Elementary reactions during which H_2 is released are primarily the formation of methyl radicals and the dehydrogenation of C_2H_6 to C_2H_4 and C_2H_4 to C_2H_2, respectively [9,21]. However, H_2 could also be released during the formation of C_3H_6 according to Eq. 3, which is proposed based on results from literature [31].

$$CH_3 + C_2H_5 \leftrightarrow C_3H_6 + H_2 \quad (3)$$

Herein, we assume that the formation of methyl radicals as well as of C_2H_5 is inhibited in the case of H_2 dilution. As the limited number of radicals reacts to C_2H_2, it seems that the reaction towards C_3H_6 is less favorable and possibly inhibited even more than the formation of C_2H_2. As depicted in Fig. 3d, Ar dilution results in significantly higher byproduct levels than H_2 dilution (Fig. 3c). The formation of C_3H_6 is a particular obstacle, as it remains stable even at higher temperatures, hereby preventing the formation of elemental carbon and gaseous H_2. Thus, we conclude that although H_2 dilution inhibits all H_2-producing elemental reactions, it promotes the H_2-selectivity.

3.2. Influence of residence time

Fig. 4 shows CH_4 conversion (Fig. 4a, b) and H_2 selectivity (Fig. 4c, d) as a function of residence time at different temperatures, constant pressure (1 bar), and constant molar dilution ratio (2:1) for H_2 and Ar as diluent gas as well as equilibrium results.

At 1100 °C and a residence time of 5 s, a CH_4 conversion of 70 % with an Ar dilution and of 30 % with a H_2 dilution is achieved. At 1200 °C, the CH_4 conversion in an Ar-diluted reaction stream is already as high as 80 % at a residence time of 1 s, whereas for H_2 as diluent the conversion is still as low as 30 %. While at equilibrium full CH_4 conversion is observed for both diluents, the difference between experimental results and equilibrium data decreases with increasing temperature. Moreover, an increasing residence time also decreases this difference and therefore promotes CH_4 conversion. This effect is however overshadowed by the temperature-induced promotion above a temperature of 1300 °C for H_2 as diluent and 1200 °C for Ar as diluent.

We attribute these results to the behavior of CH_4 activation and CH_3 radicals formation that differs in H_2 and Ar, respectively. At 1000 °C CH_4 conversion is low, thus the kinetic inhibition is surely more pronounced than a possible H_2 inhibition so that the latter one has hardly any influence. At 1100 °C and 1200 °C, both types of inhibition have a comparable effect, thus controlling the formation of CH_3 radicals. At these temperatures the advantage of an Ar dilution becomes most apparent, allowing a technical operation at a reaction temperature that is up to 100 °C lower compared to a process relying on H_2 as diluent. At 1300 °C and above, the temperature-induced acceleration of CH_4 activation outweighs the influence of the residence time as well as H_2 inhibition, therefore slightly closing the gap to the equilibrium conversion throughout the range of measured residence times. These results can be seen as complementary to previous studies, in which much lower residence times were considered [30,32,37,38].

While higher H_2 selectivities (Fig. 4c, d) can be realized for lower temperatures with argon as diluent gas, the difference is only minimal for $T \geq 1200$ °C. At 1000 °C and 1100 °C the temperature seems to be sufficient for the formation of intermediates that can be monitored end-of-pipe. Higher temperatures, as mentioned above, accelerate the reaction so much that hardly any byproducts can be detected and H_2 selectivities of above 95 % are obtained, regardless of the diluent used.

3.3. Influence of dilution ratio

Fig. 5 shows CH_4 conversion (Fig. 5a, b) and H_2 selectivity (Fig. 5c, d) as a function of the dilution ratio at different temperatures, constant residence time (5 s), and constant pressure (1 bar).

The CH_4 conversion data plotted in Fig. 5a suggest that H_2 inhibition is particularly relevant at lower temperatures, where an increase in the molar dilution ratio from 1:1–4:1 causes a significant reduction in CH_4 conversion of up to almost 40 % for experimentally determined data. Even at 1400 °C, the drop in CH_4 conversion sums up to 10 %. We attribute the inhibition by H_2 observed in our present data to a suppression of CH_3 radicals formation in the presence of high H_2 levels [19]. In contrast, increasing the dilution ratio with Ar has a positive effect on CH_4 conversion, which is most pronounced at 1000 °C but becomes less relevant at higher temperatures, since temperature effects are dominating the endothermic CH_4 pyrolysis reaction. While at 1000 °C an

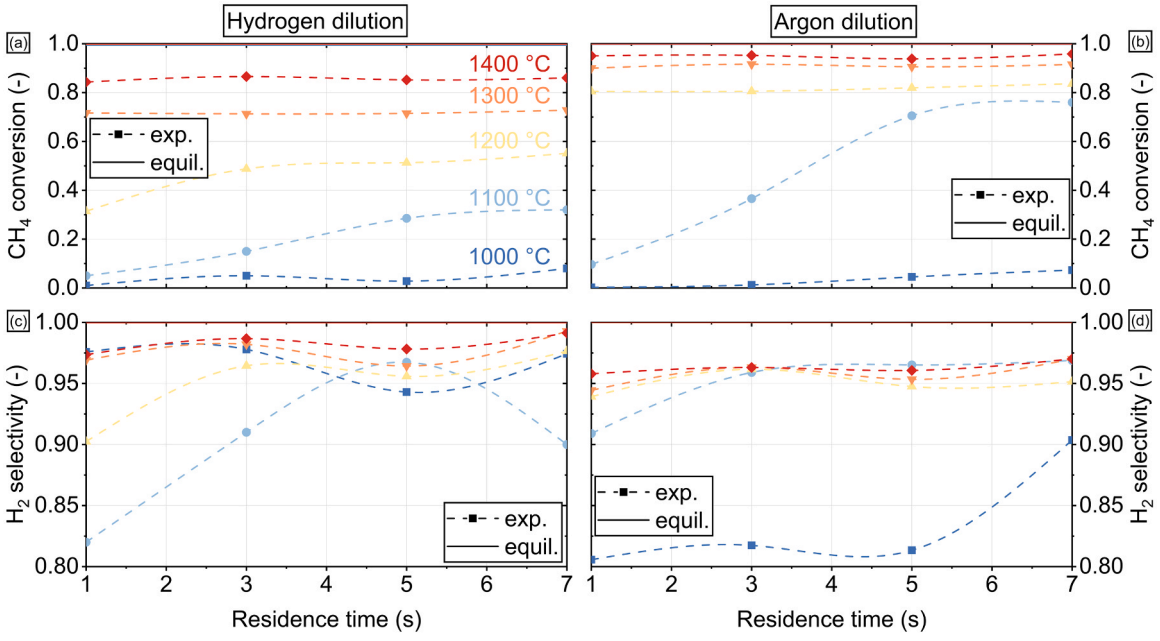

Fig. 4. Molar CH_4 conversion (a, b) and molar H_2 selectivity (c, d) for H_2 (left) or Ar (right) as dilution gas as function of residence time and temperature, at a pressure of 1 bar, and a molar dilution ratio of H_2:CH_4 = 2:1 and Ar:CH_4 = 2:1.

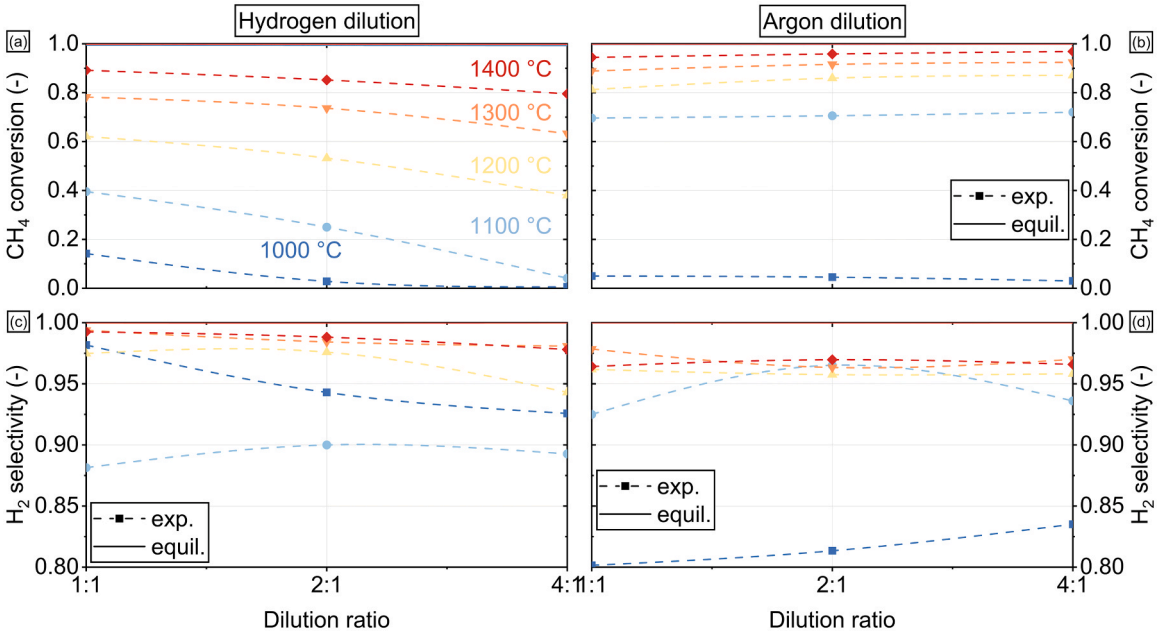

Fig. 5. Molar CH_4 conversion (a, b) and molar H_2 selectivity (c, d) for H_2 (left) or Ar (right) as dilution gas as function of dilution ratio and temperature, at a pressure of 1 bar, and a residence time of 5 s.

increase in the ratio from 1:1–4:1 increases the CH_4 conversion by 10 %, it increases only by about 5 % at 1400 °C. That increasing Ar contents benefit CH_4 decomposition is a direct consequence of the reduction in the partial pressure of methane according to Le Chatelier's principle and the associated increase in the yield of gaseous products. From a mechanistic point of view, Ar does not play a significant role in the kinetics of methane pyrolysis [29]. Irrespective of the dilution ratio, the experimental data approach the equilibrium (which is approx. 100 % for both diluents) with increasing temperature.

With regard to the H_2 selectivity, the dilution ratio is essentially almost irrelevant when using inert Ar as diluent. If H_2 is used instead, a negative effect on the H_2 selectivity is observed with increasing dilution ratio, with a less pronounced effect at higher temperatures. While at 1000 °C an increase of the ratio from 1:1–4:1 leads to a decrease of the H_2 selectivity by 15 %, hardly any difference can be observed at temperatures above 1200 °C.

As already mentioned previously, this inhibitory effect of hydrogen is described in relevant literature [30–32], however, typically lower residence times of about 0.1 s and temperatures around 1000 °C were applied. Herein, the influence of the H_2 dilution ratio on the overall reaction and on the formation of intermediates was divided into gas-phase chemistry and surface chemistry effects that come into play if carbon acts as a catalyst for hydrocarbon decomposition. While the impact of a higher amount of H_2 molecules in the gas-phase was limited, it was assumed that the H_2 molecules adsorbed on the surface of carbonaceous compounds blocked active sites and therefore caused significantly lower deposition rates. Complementary to these findings, our present results suggest that even at higher residence times and temperatures, the H_2 dilution ratio has an only limited effect on H_2 selectivity. However, to verify this suggestion, a closer look has to be taken on the product composition of minor species, which is discussed in more detail in the next section.

3.4. Influence of pressure

At first glance, the global reaction equation (Eq. 1) initially suggests that, in addition to a high temperature and a high residence time, a low pressure favors the thermal decomposition of methane according to Le Chatelier's principle. However, upon closer examination of the reaction mechanism, it seems possible that the respective elementary steps could be influenced by the pressure. Punia et al. [39] reported that the formation and further reaction of intermediates can be accelerated at higher pressures and therefore allow for higher H_2 yields compared to pressures below atmosphere. Hence, the influence of the pressure on CH_4 pyrolysis is of particular interest.

Fig. 6 shows the main product composition as a function of pressure at different temperatures, constant residence time (5 s), and constant molar dilution ratio (2:1) using either H_2 (Fig. 6a) or Ar (Fig. 6b) as diluent. Note, that the temperature-dependent trends were already discussed in the first subsection (at atmospheric pressure) and the present paragraph thus focuses on the effect of pressure.

A higher pressure has a negative effect on the CH_4 conversion for both diluent gases, whereby this effect is particularly pronounced for an H_2 dilution and becomes weaker with increasing temperature. In the case of Ar dilution, a higher pressure causes only a minimal change in the main product composition. In addition to the main products, the byproducts are of particular importance, as suppressing their formation can possibly simplify a downstream product purification in real-world pyrolysis processes. Consequently, Fig. 7 shows experimental data on the byproduct composition as a function of pressure at different temperatures, constant residence time (5 s), and constant molar dilution ratio (2:1) for H_2 (Fig. 7a) and Ar (Fig. 7b) as diluent. Note, that at these conditions the equilibrium mole fractions of the formed byproducts are negligible and therefore not shown.

As already discussed in the first subsection, C_2H_6, C_2H_4, C_2H_2, C_3H_6, and C_6H_6 are evolving for both diluent gases with a mole fraction of less than 0.6 %. In the case of H_2 dilution at atmospheric pressure, C_2H_2, C_2H_6, and C_6H_6 are the main byproducts, all with a mole fraction of less than 0.3 %. In addition, these three species have in common that they all exhibit a concentration peak at temperatures between 1200 °C and 1400 °C, as the temperatures are sufficiently high to form the intermediates, but also too low to allow the intermediates to further react in the reactor; hence, they are visible end-of-pipe [9,17].

Notably, an increase in pressure results in overall lower byproduct concentrations compared to the results at atmospheric pressure. For instance, while C_2H_2 can be detected at 1 bar for temperatures up to 1600 °C, hardly any C_2H_2 was monitored above 1300 °C when the reactor was operated at 4 bar, irrespective of the diluent. From a

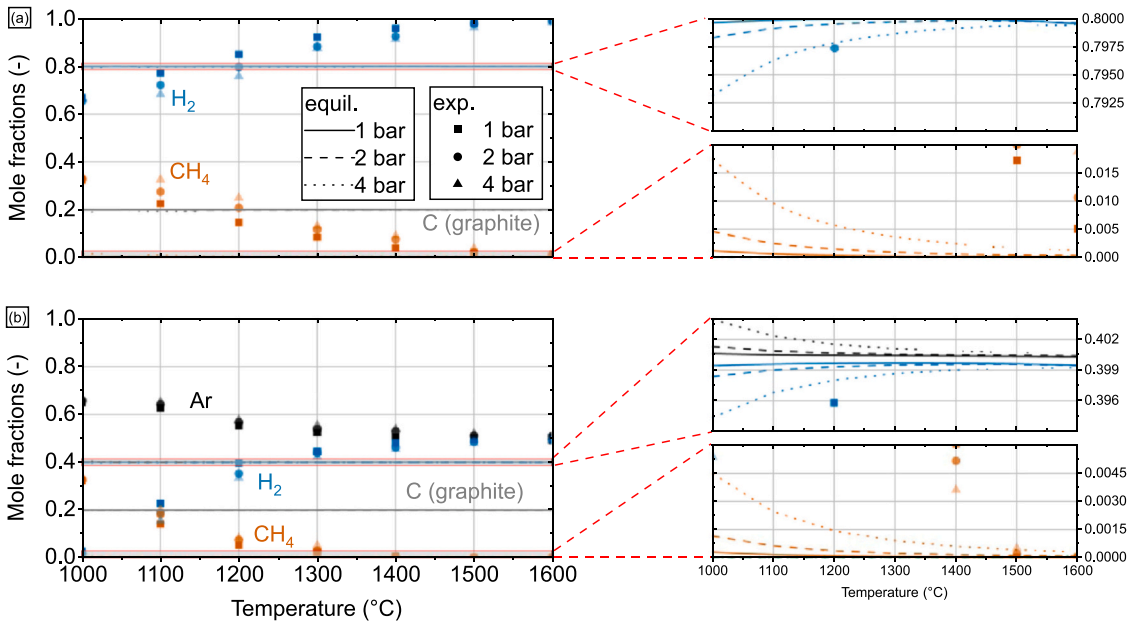

Fig. 6. Main product composition for H_2 (a) or Ar (b) as dilution gas as function of pressure and temperature, at a residence time of 5 s, and a molar dilution ratio of H_2:CH_4 = 2:1 and Ar:CH_4 = 2:1.

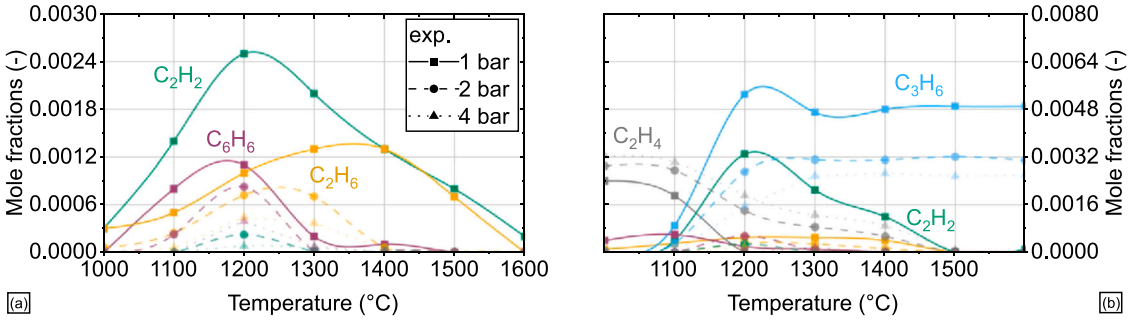

Fig. 7. Byproduct composition for H_2 (a) or Ar (b) as dilution gas as function of pressure and temperature, at a residence time of 5 s, and a molar dilution ratio of H_2: CH_4 = 2:1 and Ar:CH_4 = 2:1.

mechanistic point of view, we assume that the increased pressure suppresses the very first reaction step, namely the formation of methyl radicals. Assuming that this radical formation is the main rate limiting step [9,21], consequently also all consecutive elemental steps comprising dehydrogenation and coupling reactions [18,21] are affected. This assumption is supported by the results for the Ar-diluted gas mixture depicted in Fig. 7b. Herein, in addition to C_2H_2, C_2H_6, and C_6H_6 (all with comparable mole fractions to a H_2 dilution), also C_2H_4 (with mole fractions between 0.2 % and 0.3 %) and especially C_3H_6 (with mole fractions between 0.3 % and 0.6 %) can be observed. While a diluent variation results in qualitatively similar trends for C_2H_2, C_2H_6, and C_6H_6, the mole fraction curves of C_2H_4 and C_3H_6 at different pressure differ strongly.

Moreover, the mole fraction of C_2H_4 is increasing at higher pressures for an Ar-diluted gas mixture (Fig. 7b). One possible reason for the increased C_2H_4 levels, could be a re-hydrogenation of C_2H_2 to C_2H_4, which would also explain why almost no C_2H_2 can be observed end-of-pipe for a pressure of 2 bar and above, irrespective of the temperature. In comparison to an H_2 dilution, where C_2H_4 is hardly present, this could conversely mean that H_2 not only influences the methyl radical formation, but also impacts any reaction resulting in ethylene formation.

Also C_3H_6 formation, which can only be observed in the case of Ar dilution, is strongly influenced by the H_2 presence and the pressure. Its formation starts at a temperature of 1100 °C and the C_3H_6 molar fraction reaches a plateau at 1300 °C and above. Note, that the absolute level of this C_3H_6 concentration plateau decreases with rising pressure, in particular from a fraction of approx. 0.48 % at 1 bar to approx. 0.2 % at 4 bar.

Since C_3H_6 is most likely formed from CH_3 and C_2H_5 radicals (c.f. Eq. 3) [31], the addition of H_2 seems to inhibit this reaction twofold: First, by inhibiting CH_3 radical formation and second, according to Le Chatelier's principle as H_2 is a byproduct of C_3H_6 formation. However, as the reaction is equimolar, an impact of a pressure increase is not expected. We attribute this to an inhibition of CH_3 radical formation in the first place as well. According to reaction flow analyses conducted previously by our group [9,21], C_2H_5 is strongly needed for C_2H_2 and subsequent C_6H_6 and solid compounds formation. Therefore, the formation of C_3H_6 is a dead-end for the reaction system, which also explains its presence even at temperatures as high as 1600 °C. As a summary, a schematic simplified overview of the reaction network for H_2- and Ar-diluted reaction gas mixtures under the conditions applied in the present study is given in Fig. 8.

4. Conclusions

Our work studies the thermal pyrolysis of methane at high temperatures, in particular the impact of the two different dilution gases hydrogen and inert argon, by means of experimental investigations and

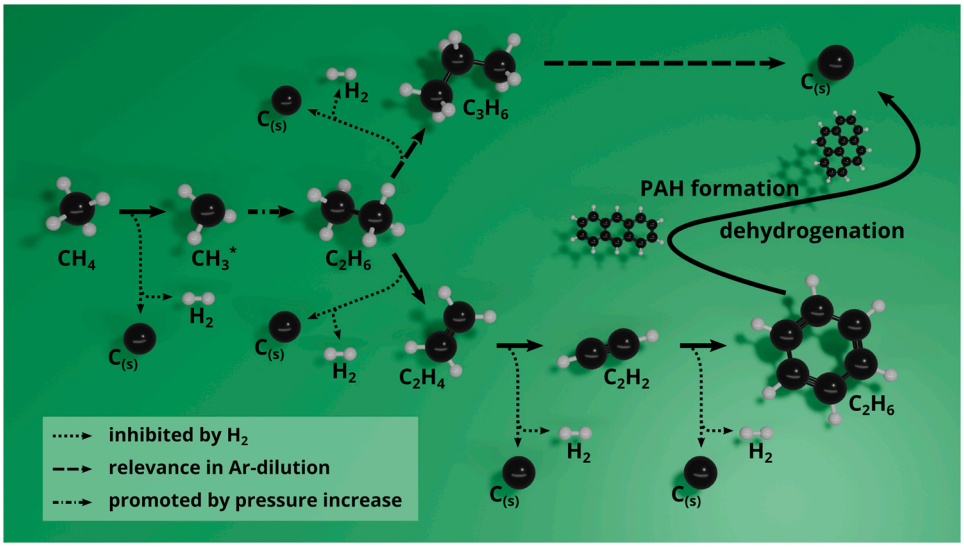

Fig. 8. Simplified reaction network for H_2- and Ar-diluted reaction gas mixtures as subject to the present study.

corresponding thermodynamic equilibrium data. Herein, we clarified the inhibitory effect of H_2 on the reaction by analyzing the influence of the process parameters temperature, residence time, molar dilution ratio, and pressure on the product composition, the CH_4 conversion, and the H_2 selectivity.

Overall, using H_2 as diluent results in a strong inhibition of CH_4 conversion. For instance, at 1100 °C, a residence time of 7 s, and a dilution ratio of 2:1, a CH_4 conversion of 80 % can be achieved with an Ar dilution, whereas only 30 % CH_4 conversion are achieved with a H_2 dilution. Especially at temperatures between 1000 °C and 1200 °C, a higher dilution with argon leads to a lower partial pressure of methane, which promotes CH_4 conversion. Notably, the H_2 inhibition effect becomes less relevant as the temperature increases while approaching equilibrium performance at temperatures above 1400 °C with both dilution gases. However, H_2 dilution suppresses the formation of undesired byproducts, that sum up to a maximum of 1 % in Ar dilution under the most disadvantageous reaction conditions ($T = 1200$ °C, $\tau = 5$ s, $p =$ 1 bar), to a significant extent. A further reduction of the byproduct levels is possible if the methane pyrolysis reactor is operated under pressure: An increase in pressure from 1 bar to 4 bar has an only marginal effect on CH_4 conversion, but reduces the formation of byproducts significantly for both H_2 and Ar as diluent. While in the best case this leads to a cumulated total concentration of C_2-hydrocarbons and C_6H_6 as low as 0.05 % for a H_2-diluted reaction gas mixture ($T > 1200$ °C, $\tau = 5$ s, $p =$ 4 bar), the total byproduct concentration exceeds 0.2 % if Ar is used as diluent instead. In addition, significant amounts of C_3H_6 are formed in Ar-diluted reaction gas mixtures, presumably due to a reaction between CH_3 and C_2H_5 radicals. Since C_3H_6 is present even at high pressures and temperatures as high as 1600 °C, it has to be considered as an obstacle that impedes full decomposition of CH_4 to form solid carbon and gaseous H_2.

While additional experiments and numerical simulations, preferentially with spatially resolved information on species and temperature profiles, are desirable to further substantiate such hypotheses, the current study underscores the importance of choosing suitable dilution ratios and diluent gases. In the end, techno-economic considerations will allow to decide whether an increased CH_4 conversion in Ar-diluted gas streams at lower temperatures but with higher byproduct levels and an energy-intensive product gas separation unit is most desirable, or if H_2-diluted gas streams that ensure high product selectivity at comparably high reactor temperatures should be chosen instead.

Funding sources

This research did not receive any specific grant from funding agencies in the public, commercial, or not-for-profit sectors.

CRediT authorship contribution statement

Ahmet Çelik: Writing – original draft, Visualization, Validation, Methodology, Investigation, Formal analysis, Data curation, Conceptualization. **Akash Bhimrao Shirsath**: Formal analysis, Investigation, Software, Validation. **Fatjon Syla**: Investigation, Formal analysis. **Heinz Müller**: Investigation, Formal analysis, Data curation. **Patrick Lott**: Writing – original draft, Project administration, Conceptualization, Data curation, Methodology, Supervision, Visualization. **Olaf Deutschmann**: Writing – review & editing, Supervision, Resources, Project administration, Conceptualization, Data curation.

Declaration of Competing Interest

The authors declare that they have no known competing financial interests or personal relationships that could have appeared to influence the work reported in this paper.

Data availability

Data will be made available on request.

Acknowledgements

We thank M. Berg and C. Kroll (Berg-idl GmbH) for their support in engineering the high-temperature vessel of the experimental setup, S. Lichtenberg (KIT) for technical support, and S. Tischer (KIT) for fruitful discussion.

Appendix A. Supporting information

Supplementary data associated with this article can be found in the online version at doi:10.1016/j.jaap.2024.106628.

References

[1] M. Hermesmann, T.E. Müller, Green, turquoise, blue, or grey? Environmentally friendly hydrogen production in transforming energy systems, Prog. Energy Combust. Sci. 90 (2022) 100996, https://doi.org/10.1016/j.pecs.2022.100996.

[2] J. Hwang, K. Maharjan, H. Cho, A review of hydrogen utilization in power generation and transportation sectors: achievements and future challenges, Int. J. Hydrogen Energy 48 (2023) 28629–28648, https://doi.org/10.1016/j.ijhydene.2023.04.024.

[3] P. Lott, O. Deutschmann, Heterogeneous chemical reactions - a cornerstone in emission reduction of local pollutants and greenhouse gases, Proc. Combust. Inst. 39 (2023) 3183–3215, https://doi.org/10.1016/j.proci.2022.06.001.

[4] V.M. Maestre, A. Ortiz, I. Ortiz, Challenges and prospects of renewable hydrogen-based strategies for full decarbonization of stationary power applications, Renewable Sustainable Energy Rev. 152 (2021) 111628, https://doi.org/10.1016/j.rser.2021.111628.

[5] B. Parkinson, M. Tabatabaei, D.C. Upham, B. Ballinger, C. Greig, S. Smart, E. McFarland, Hydrogen production using methane: techno-economics of decarbonizing fuels and chemicals, Int. J. Hydrogen Energy 43 (2018) 2540–2555, https://doi.org/10.1016/j.ijhydene.2017.12.081.

[6] M.G. Rasul, M.A. Hazrat, M.A. Sattar, M.I. Jahirul, M.J. Shearer, The future of hydrogen: challenges on production, storage and applications, Energy Convers. Manage. 272 (2022) 116326, https://doi.org/10.1016/j.enconman.2022.116326.

[7] M. Younas, S. Shafique, A. Hafeez, F. Javed, F. Rehman, An overview of hydrogen production: current status, potential, and challenges, Fuel 316 (2022) 123317, https://doi.org/10.1016/j.fuel.2022.123317.

[8] T.I. Korányi, M. Németh, A. Beck, A. Horváth, Recent advances in methane pyrolysis: turquoise hydrogen with solid carbon production, Energies 15 (2022) 6342, https://doi.org/10.3390/en15176342.

[9] P. Lott, M.B. Mokashi, H. Müller, D.J. Heitlinger, S. Lichtenberg, A.B. Shirsath, C. Janzer, S. Tischer, L. Maier, O. Deutschmann, Hydrogen production and carbon capture by gas phase methane pyrolysis: a feasibility study, ChemSusChem 16 (2023) e202201720, https://doi.org/10.1002/cssc.202201720.

[10] O. Machhammer, A. Bode, W. Hormuth, Financial and ecological evaluation of hydrogen production processes on large scale, Chem. Eng. Technol. 39 (2016) 1185–1193, https://doi.org/10.1002/ceat.201600023.

[11] N. Muradov, Low to near-zero CO_2 production of hydrogen from fossil fuels: status and perspectives, Int. J. Hydrogen Energy 42 (2017) 14058–14088, https://doi.org/10.1016/j.ijhydene.2017.04.101.

[12] N. Muradov, T. Veziroğlu, From hydrocarbon to hydrogen–carbon to hydrogen economy, Int. J. Hydrogen Energy 30 (2005) 225–237, https://doi.org/10.1016/j.ijhydene.2004.03.033.

[13] D. Nativel, B. Shu, J. Herzler, M. Fikri, C. Schulz, Shock-tube study of methane pyrolysis in the context of energy-storage processes, Proc. Combust. Inst. 37 (2019) 197–204, https://doi.org/10.1016/j.proci.2018.06.083.

[14] S.R. Patlolla, K. Katsu, A. Sharafian, K. Wei, O.E. Herrera, W. Mérida, A review of methane pyrolysis technologies for hydrogen production, Renewable Sustainable Energy Rev. 181 (2023) 113323, https://doi.org/10.1016/j.rser.2023.113323.

[15] N. Sánchez-Bastardo, R. Schlögl, H. Ruland, Methane pyrolysis for CO_2-free H_2 production: A green process to overcome renewable energies unsteadiness, Chem. Ing. Tech. 92 (2020) 1596–1609, https://doi.org/10.1002/cite.202000029.

[16] S. Schneider, S. Bajohr, F. Graf, T. Kolb, State of the art of hydrogen production via pyrolysis of natural gas, ChemBioEng Rev. 7 (2020) 150–158, https://doi.org/10.1002/cben.202000014.

[17] A. Çelik, I. Ben Othman, H. Müller, P. Lott, O. Deutschmann, Pyrolysis of biogas for carbon capture and carbon dioxide-free production of hydrogen, React. Chem. Eng. 9 (2024) 108–118, https://doi.org/10.1039/d3re00360d.

[18] J. Appel, H. Bockhorn, M. Frenklach, Kinetic modeling of soot formation with detailed chemistry and physics: laminar premixed flames of C_2 hydrocarbons, Combust. Flame 121 (2000) 122–136, https://doi.org/10.1016/s0010-2180(99)00135-2.

[19] M. Frenklach, Reaction mechanism of soot formation in flames, Phys. Chem. Chem. Phys. 4 (2002) 2028–2037, https://doi.org/10.1039/b110045a.

[20] A. Holmen, O. Olsvik, O.A. Rokstad, Pyrolysis of natural gas: chemistry and process concepts, Fuel Process. Technol. 42 (1995) 249–267, https://doi.org/10.1016/0378-3820(94)00109-7.

[21] M. Mokashi, A.B. Shirsath, P. Lott, H. Müller, S. Tischer, L. Maier, O. Deutschmann, Understanding of gas-phase methane pyrolysis towards hydrogen and solid carbon with detailed kinetic simulations and experiments, Chem. Eng. J. 479 (2024) 147556, https://doi.org/10.1016/j.cej.2023.147556.

[22] K. Norinaga, O. Deutschmann, N. Saegusa, J.-I. Hayashi, Analysis of pyrolysis products from light hydrocarbons and kinetic modeling for growth of polycyclic aromatic hydrocarbons with detailed chemistry, J. Anal. Appl. Pyrolysis 86 (2009) 148–160, https://doi.org/10.1016/j.jaap.2009.05.001.

[23] K. Norinaga, O. Deutschmann, Detailed kinetic modeling of gas-phase reactions in the chemical vapor deposition of carbon from light hydrocarbons, Ind. Eng. Chem. Res. 46 (2007) 3547–3557, https://doi.org/10.1021/ie061207p.

[24] A.B. Shirsath, M. Mokashi, P. Lott, H. Müller, R. Pashminehazar, T. Sheppard, S. Tischer, L. Maier, J.-D. Grunwaldt, O. Deutschmann, Soot formation in methane pyrolysis reactor: modeling soot growth and particle characterization, J. Phys. Chem. A 127 (2023) 2136–2147, https://doi.org/10.1021/acs.jpca.2c06878.

[25] T. Keipi, K.E.S. Tolvanen, H. Tolvanen, J. Konttinen, Thermo-catalytic decomposition of methane: the effect of reaction parameters on process design and the utilization possibilities of the produced carbon, Energy Convers. Manage. 126 (2016) 923–934, https://doi.org/10.1016/j.enconman.2016.08.060.

[26] L. Zhou, L.R. Enakonda, M. Harb, Y. Saih, A. Aguilar-Tapia, S. Ould-Chikh, J.-L. Hazemann, J. Li, N. Wei, D. Gary, P. Del-Gallo, J. Basset, Fe catalysts for methane decomposition to produce hydrogen and carbon nano materials, Appl. Catal., B 208 (2017) 44–59, https://doi.org/10.1016/j.apcatb.2017.02.052.

[27] S.H. Sharif Zein, A.R. Mohamed, P.S. Talpa Sai, Kinetic studies on catalytic decomposition of methane to hydrogen and carbon over Ni/TiO_2 catalyst, Ind. Eng. Chem. Res. 43 (2004) 4864–4870, https://doi.org/10.1021/ie034208f.

[28] A. Sheil, M. Konarova, M. McConnachie, S. Smart, Selectivity and reaction kinetics of methane pyrolysis to produce hydrogen in catalytically active molten salts, Appl. Energy 364 (2024) 123137, https://doi.org/10.1016/j.apenergy.2024.123137.

[29] O.A. Rokstad, O. Olsvik, B. Jenssen, A. Holmen, L.F. Albright, B.L. Crynes, S. Nowak, Novel production methods for ethylene. light hydrocarbons, and aromatics, M. Dekker New York, 1992.

[30] A. Becker, K.J. Hüttinger, Chemistry and kinetics of chemical vapor deposition of pyrocarbon — II pyrocarbon deposition from ethylene, acetylene and 1,3-butadiene in the low temperature regime, Carbon 36 (1998) 177–199, https://doi.org/10.1016/s0008-6223(97)00175-9.

[31] A. Becker, K.J. Hüttinger, Chemistry and kinetics of chemical vapor deposition of pyrocarbon — III pyrocarbon deposition from propylene and benzene in the low temperature regime, Carbon 36 (1998) 201–211, https://doi.org/10.1016/s0008-6223(97)00176-0.

[32] W. Benzinger, A. Becker, K.J. Hüttinger, Chemistry and kinetics of chemical vapour deposition of pyrocarbon: I. Fundamentals of kinetics and chemical reaction engineering, Carbon 34 (1996) 957–966, https://doi.org/10.1016/0008-6223(96)00010-3.

[33] S.D. Angeli, S. Gossler, S. Lichtenberg, G. Kass, A.K. Agrawal, M. Valerius, K. P. Kinzel, O. Deutschmann, Reduction of CO_2 emission from off-gases of steel industry by dry reforming of methane, Angew. Chem., Int. Ed. 60 (2021) 11852–11857, https://doi.org/10.1002/anie.202100577.

[34] M. Mokashi, A.B. Shirsath, A. Çelik, P. Lott, H. Müller, S. Tischer, L. Maier, J. Bode, D. Schlereth, F. Scheiff, D. Flick, M. Bender, K. Ehrhardt, O. Deutschmann, Methane pyrolysis in packed bed reactors: kinetic modeling, numerical simulations, and experimental insights, Chem. Eng. J. 485 (2024) 149684, https://doi.org/10.1016/j.cej.2024.149684.

[35] O. Deutschmann, S. Tischer, S. Kleditzsch, V. Janardhanan, C. Correa, D. Chatterjee, N. Mladenov, H.D. Minh, H. Karadeniz, M. Hettel, V. Menon, A. Banerjee, H. Gossler, A.B. Shirsath, E. Daymo, DETCHEM Software package, 2.9 ed., www.detchem.com, Karlsruhe (2022).

[36] A. Burcat (Technion Israel Institute of Technology) Ideal Gas Thermodynamic Data in Polynomial form for Combustion and Air Pollution Use, http://garfield.chem.elte.hu/Burcat/burcat.html (Access: May 16, 2024).

[37] F. Billaud, C. Gueret, J. Weill, Thermal decomposition of pure methane at 1263 K. Experiments and mechanistic modelling, Thermocim. Acta 211 (1992) 303–322, https://doi.org/10.1016/0040-6031(92)87029-a.

[38] O. Olsvik, O.A. Rokstad, A. Holmen, Pyrolysis of methane in the presence of hydrogen, Chem. Eng. Technol. 18 (1995) 349–358, https://doi.org/10.1002/ceat.270180510.

[39] A. Punia, J. Tatum, L. Kostiuk, J. Olfert, M. Secanell, Analysis of methane pyrolysis experiments at high pressure using available reactor models, Chem. Eng. J. 471 (2023) 144183, https://doi.org/10.1016/j.cej.2023.144183.